Appendix from "Predation as an explanation for a latitudinal gradient in arm number among featherstars"

Features of the dataset

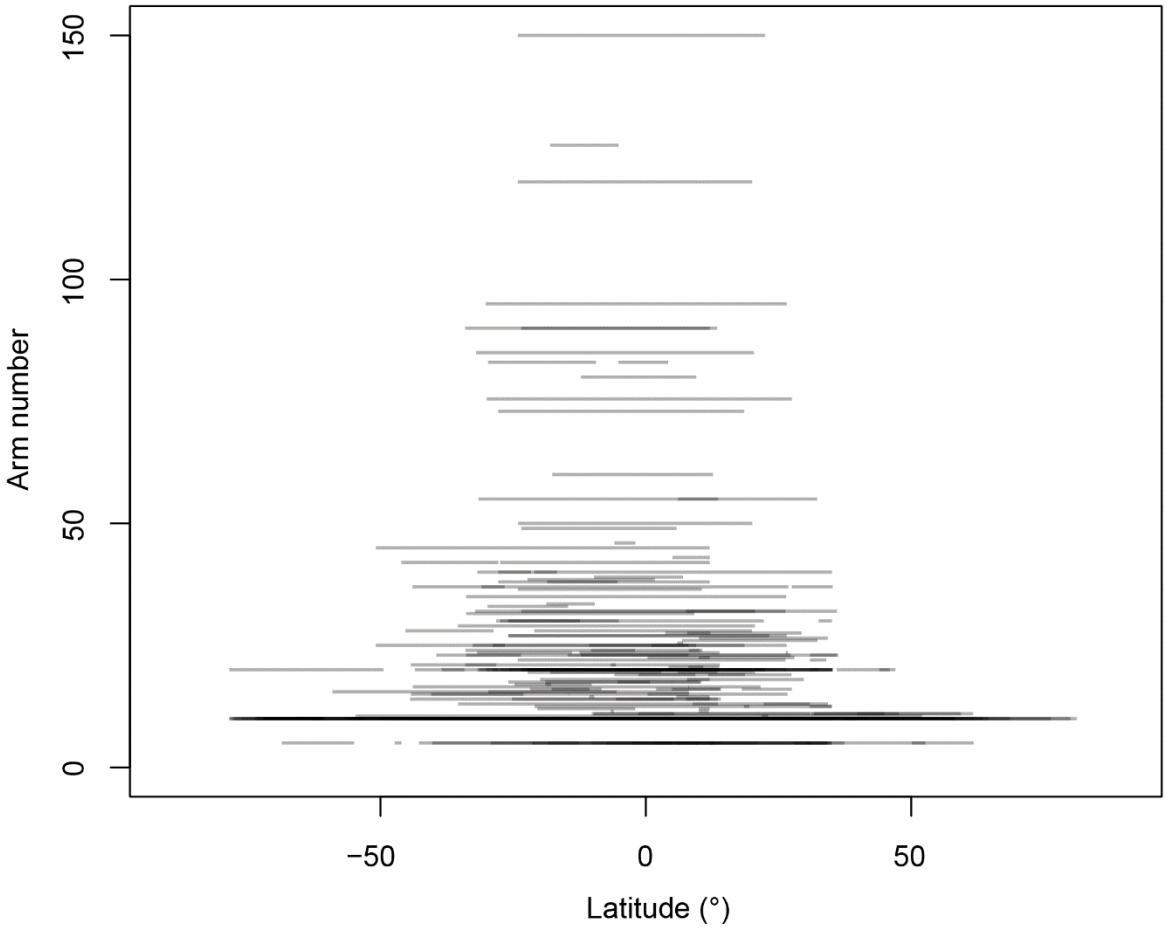

Fig. A1. The latitudinal range and arm number of all 442 species in the dataset, plotted at 40% opacity.

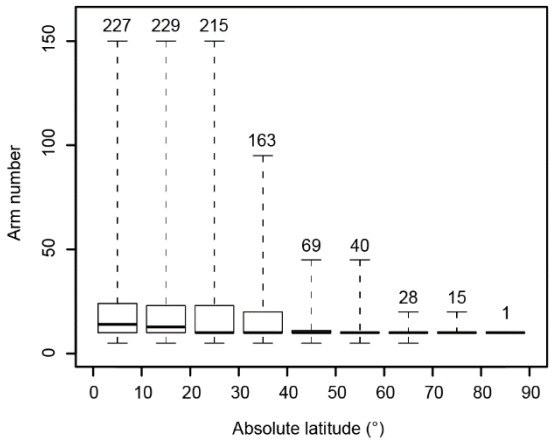

Fig A2. Arm number distribution for species whose latitudinal range includes each 10° band of absolute latitude. The number of species in each band is indicated above each boxplot.

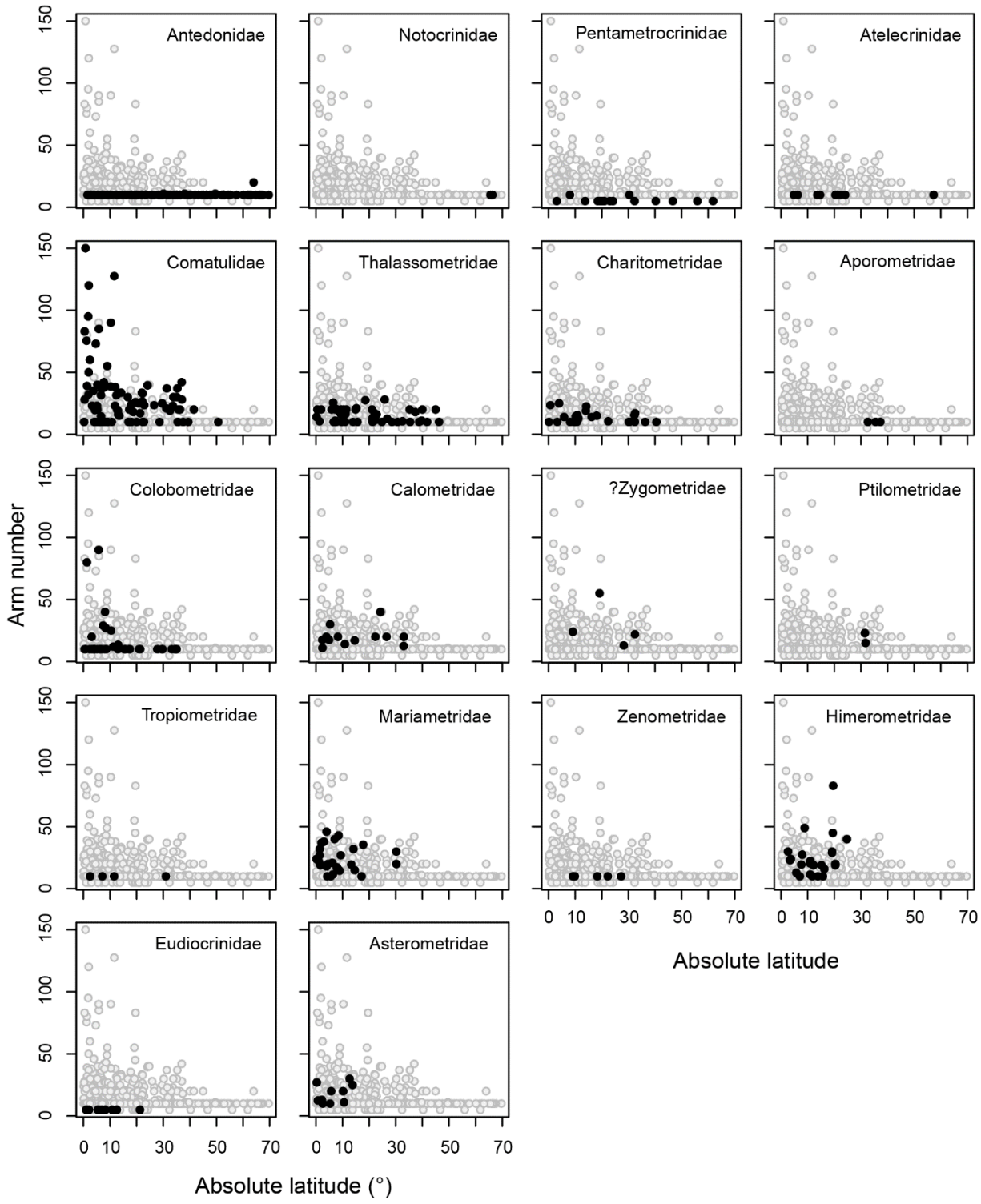
Antedonidae
Notocrinidae
Pentametrocrinidae
Atelecrinidae
Comatulidae
Thalassometridae
Charitometridae
Aporometridae
Colobometridae
Calometridae
?Zygometridae
Ptilometridae
Tropiometridae
Mariametridae
Zenometridae
Himerometridae
Eudiocrinidae
Asterometridae
Arm number
0 50 100 150
0 10 30 50 70
Absolute latitude
Absolute latitude (°)

11

Fig. A3. Latitude-arm number relationships within all families. "?Zygometridae" comprises only the genus *Catoptometra*, whose phylogenetic affinity has recently been thrown into question (Taylor 2015).

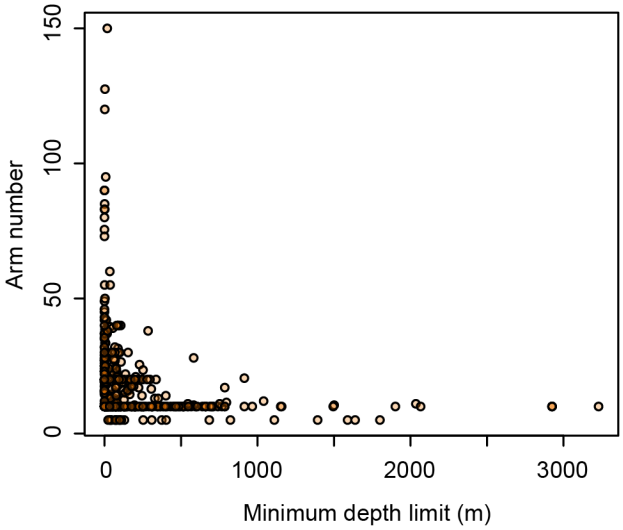

Fig. A4. The shallowest depth observed for by each featherstar species, plotted against their arm number. No featherstar species with more than 40 arms has their shallowest occurrence below shelf depths.

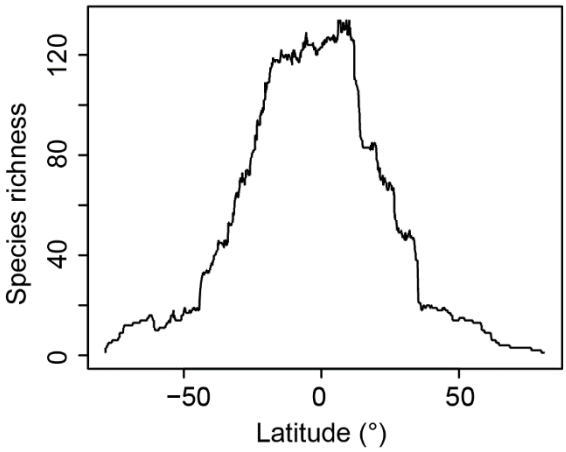

Fig. A5. Another view of the latitudinal diversity gradient among featherstars: the number of species present at every latitude. The number of species in each 10° latitudinal bin can be seen in Fig. A2.

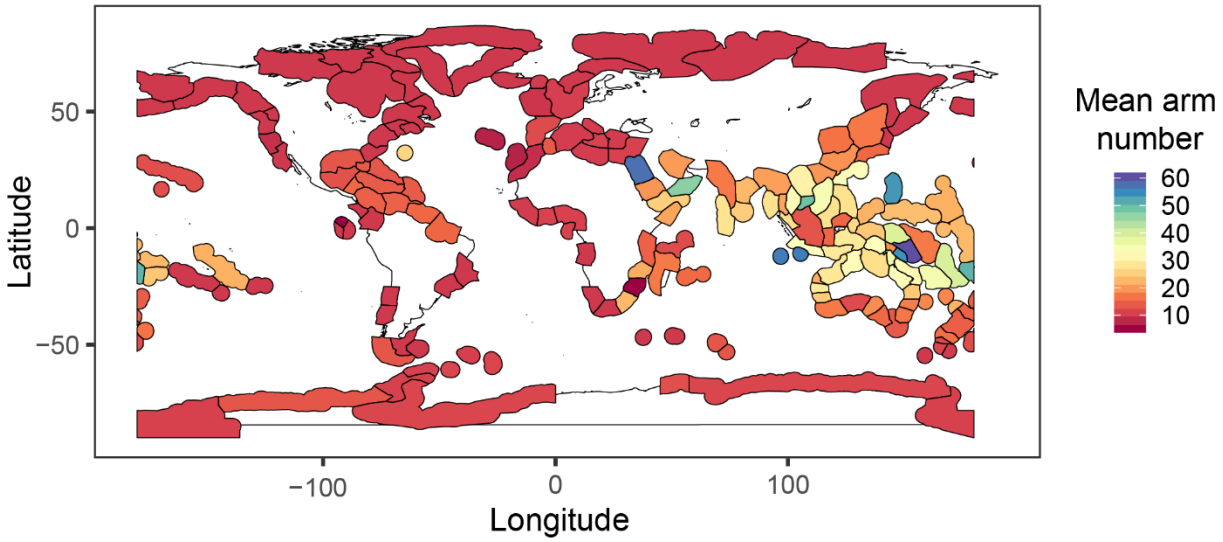

Fig. A6. Mean arm number of species with occurrences in each of 232 shallow marine ecoregions following Spalding et al. (2007). Note that many deep-sea occurrences are not shown here.

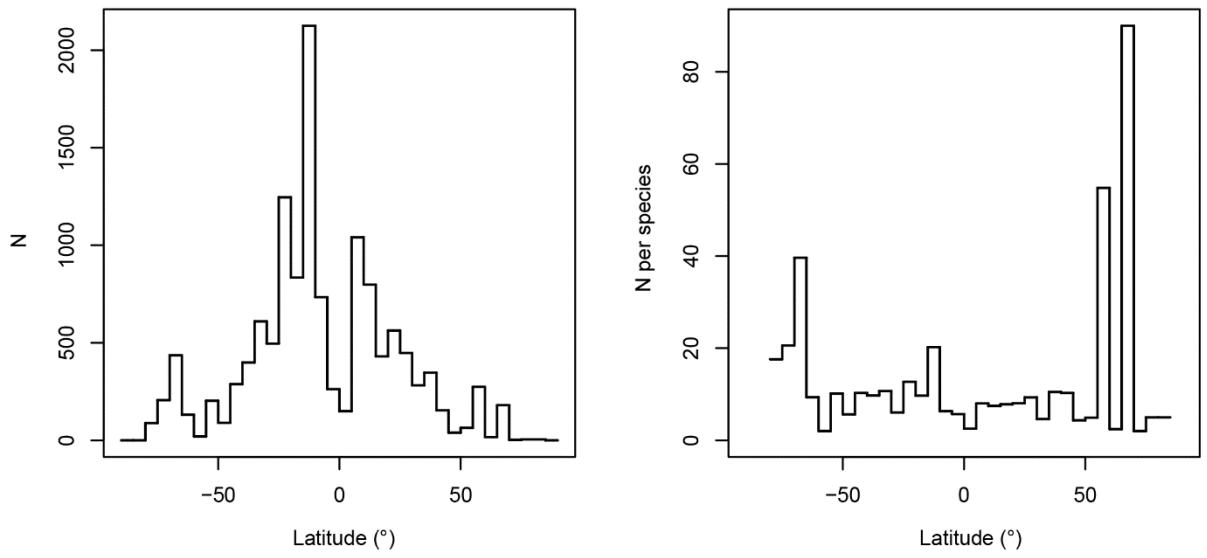

Fig. A7. Sampling across latitude. Left, the number of occurrences in each 5° latitudinal band. Right: the average number of occurrences per species in each latitudinal band. The plot on the right excludes the 8 species with more than 400 occurrences.

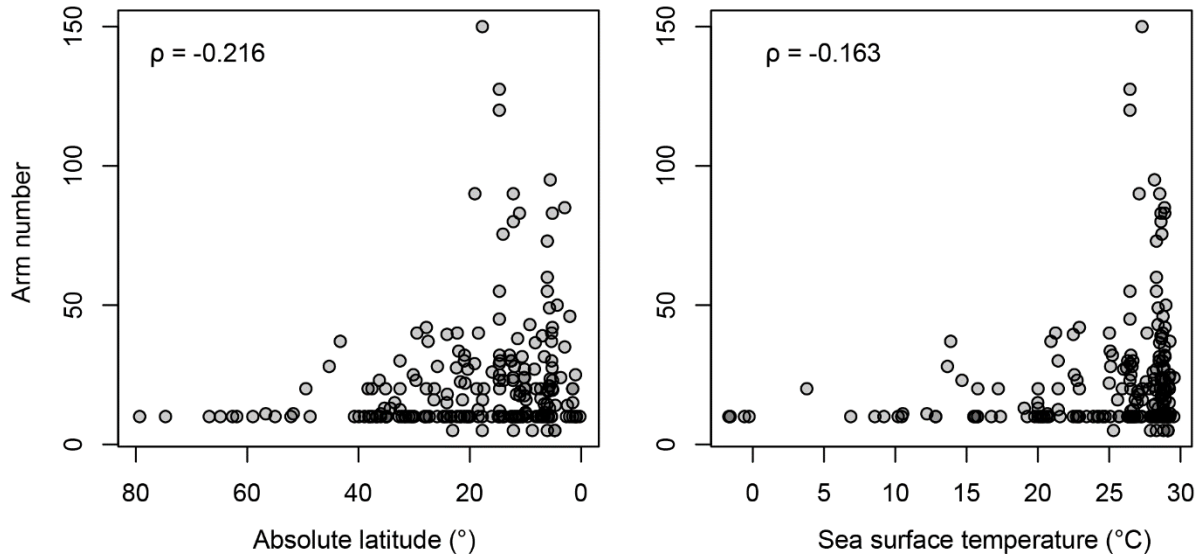

Fig. A8. Temperature and latitude against arm number, with a single paired observation of latitude and temperature randomly chosen for each species.

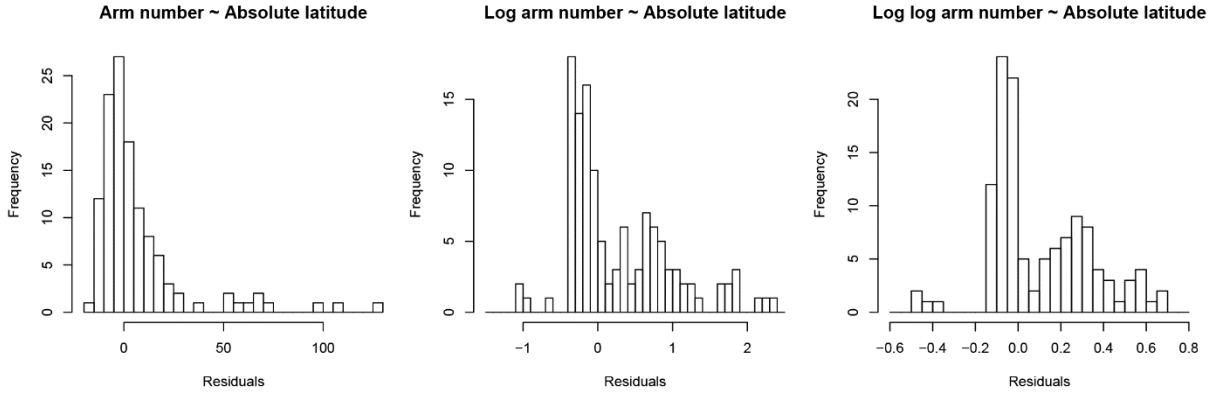

Fig. A9. Histograms showing the distribution of residuals in separate PGLS regressions of arm number, log arm number, and log log arm number on absolute latitude.

Chronogram

We scaled the molecular phylogeny of featherstars inferred by Saulsbury and Zamora (2019) to units of time using Sanderson's (2002) penalized likelihood approach. Penalized likelihood balances a clocklike, nonparametric picture of sequence evolution, in which all branches of the tree share one substitution rate, with a "saturated" model in which each branch is parameterized by its own rate. Higher values of a smoothing parameter λ up-weight the clocklike term in the penalized likelihood equation. Leave-one-out cross-validation, as implemented in the penalized likelihood software package *treePL* (Smith and O'Meara 2012) reveals that the age of dropped tips in our phylogeny is best predicted when λ is close to 0; in other words, the molecular data are not very clock-like.

Dates for fossil calibrations follow the International Commission on Stratigraphy's Chronostratigraphic Chart v. 2019/05 (Cohen et al. 2013). Fossil featherstars (whose positions within the stem or crown are unknown) are recorded from the Hettangian (Jurassic), and we somewhat arbitrarily set the root of the tree at the base of the Jurassic (201.3 Ma). Two additional nodes were constrained based on fossil information. A minimum age of 20.44 Ma was assigned to the node uniting Comatulidae and Thalassometridae, corresponding to the end of the Aquitanian stage of the Miocene. *Comaster formae* from the Aquitanian of Italy represents a definitive member of the Comatulidae (Hess and Messing 2011). The node uniting Himerometroidea to the exclusion of all other featherstars was assigned a minimum age of 33.9 Ma based on the fossil himerometrid *Himerometra bassleri* from the Eocene of South Carolina (Gislen 1934).

Phylogenetic permutations

Here we expand on the new approach of phylogenetic permutations, dealing with details of generating the distribution of permutations and explaining a test of the approach with Felsenstein's "worst case" scenario. All statistics calculated for the set of phylogenetic permutations (Spearman's ρ and the slopes of the 90th and 95th conditional percentiles) had greater variance than statistics for a set of ordinary permutations, with $p < 0.001$ in all cases and ratios of variance between 1.19 and 1.46 (Fig. A9). However, unlike in Felsenstein's worst case (Fig. A13), the distribution of statistics for phylogenetic and ordinary permutations were visually similar, suggesting that the moderate phylogenetic signal in the data did not convey a strong tendency to induce spurious correlations. The hill-climbing algorithm used to generate phylogenetic permutations permutes and then iteratively tries to swap pairs of values, accepting swaps if the new phylogenetic signal is as close or closer to the empirical signal. One statistical issue with this algorithm is that if it searches the space of possible permutations in a biased way, the p-value based on the set of phylogenetic permutations could be misleading. This is worth exploring further, but here we merely emphasize that none of the phylogenetic permutations of either the predictor or response variable were duplicates.

The statistics associated with nulls differed slightly when the predictor, response variable, or both were phylogenetically permuted (Fig. A11). P-values are similar regardless of choice, but we presented permutations of both predictor and response in the main text. Phylogenetic permutations generated with Blomberg's K and Pagel's lambda had statistically indistinguishable variances for the slopes of the 90th and 95th conditional percentiles, but Spearman's ρ had greater variance for Blomberg's K. (Fig. A12). Thus, using Blomberg's K is either more conservative than

or statistically indistinguishable from using Pagel's λ. The latter was also much slower to converge on the empirical phylogenetic signal because for most configurations the signal was near zero. For this reason we used Blomberg's K in all other analyses.

In Felsenstein's (1985) "worst case" scenario, two traits that evolved independently are spuriously correlated with one another due to the structure of the phylogeny on which they evolved. This scenario was used to motivate the development of methods robust to the effects of phylogenetic autocorrelation. We simulated the evolution of two traits, x and y, by Brownian motion on a tree in which two polytomous clades of 20 taxa are subtended by branches half the height of the phylogeny (Fig. A13A). The effect size of a regression of y on x ($r^2 = 0.12$, $p < 0.001$) was compared with that of ordinary (Fig. A13B) and phylogenetic permutations (Fig. A13C). This "empirical" effect size was significantly greater than in 99.6% of ordinary permutations, but only greater than 10.1% of phylogenetic permutations (Fig. A13D). Thus, almost every rearrangement of the traits on the tree that retains the high phylogenetic signal of those traits generates a spurious correlation between x and y. In other words, the phylogenetic permutation approach succeeds in demonstrating that the apparent correlation between traits in Felsenstein's worst case is merely a result of phylogenetic autocorrelation. Note that, unlike in the independent contrasts approach, phylogenetic permutations could be used to investigate the distribution of any test statistic that could be applied to x and y.

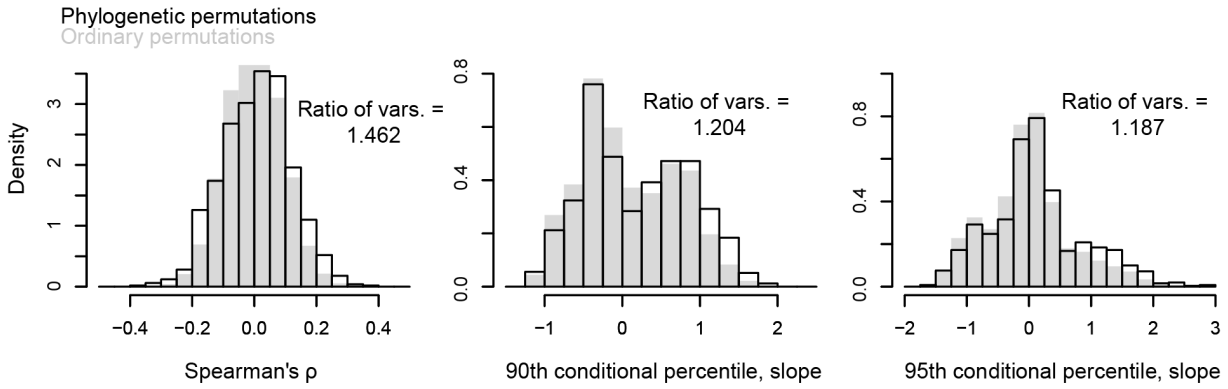

105

106 **Fig. A10.** Visual and statistical comparison of statistics associated with ordinary and phylogenetic
107 permutations. Shown as density because 10,000 ordinary permutations are shown, compared with
108 just 1000 phylogenetic permutations. All variance tests significant at the $p < 0.0005$ level.

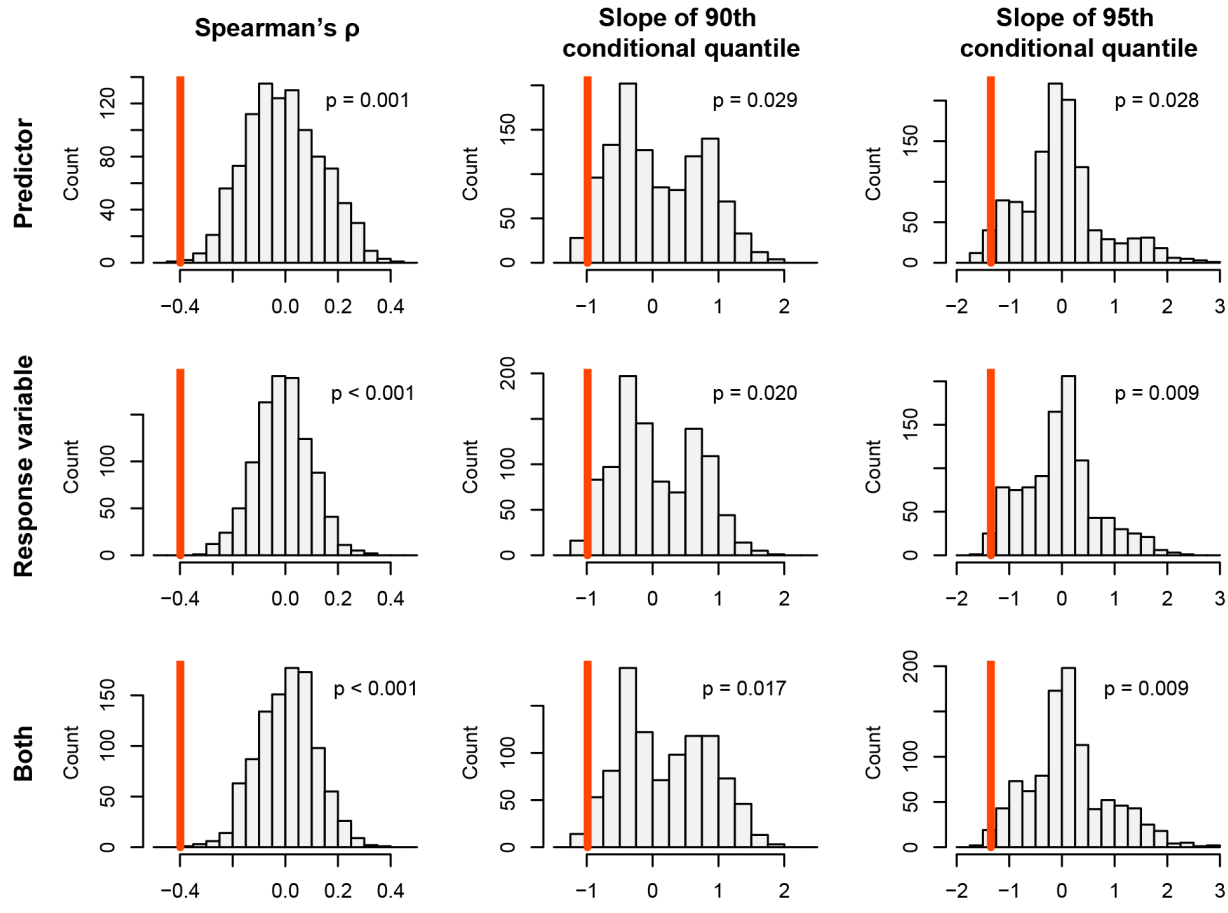

109

Fig. A11. Results of phylogenetic permutations of the predictor (absolute latitude), response variable (arm number), and both. The vertical orange bar indicates the empirical value of a given statistic. 1000 permutations were generated for each row.

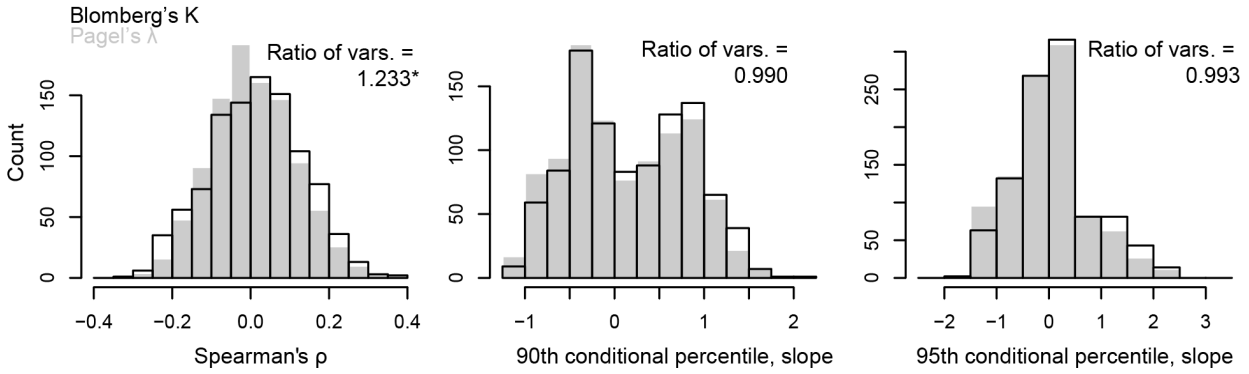

Fig. A12. Comparison of phylogenetic permutations generated using Blomberg's K (dark lines) and Pagel's λ (solid grey). Asterisk indicates statistical significance ($p < 0.001$ for the leftmost test).

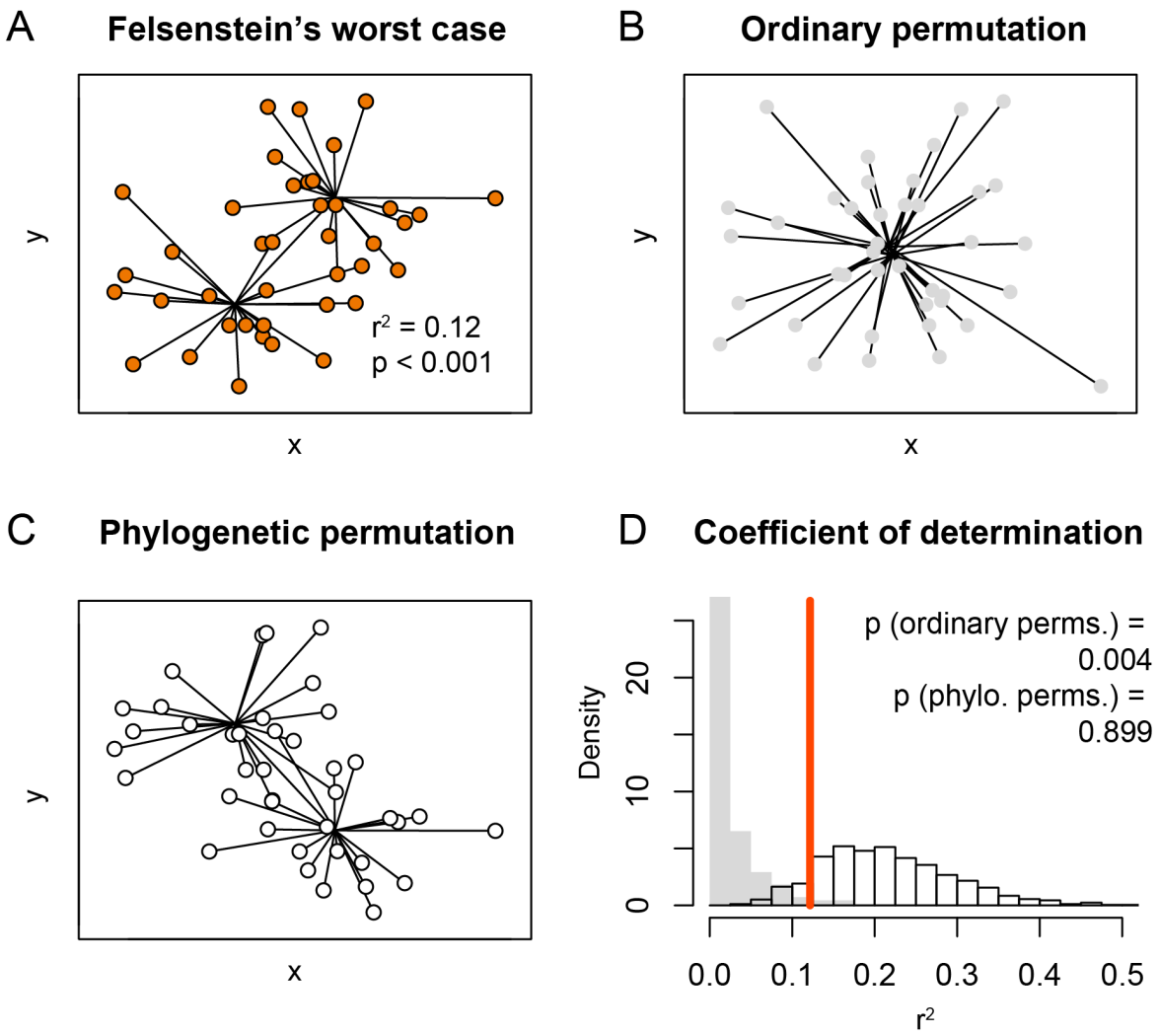

Fig. A13. Applying phylogenetic permutations to Felsenstein's "worst case." *A*, two traits x and y simulated on a phylogeny [(Felsenstein 1985, Fig. 5)]. Values of internal nodes represent ancestral state reconstructions. *B*, The same phylogeny and set of traits, with both x and y permuted (labels on data shuffled randomly). *C*, The same phylogeny and set of traits, but with both traits phylogenetically permuted to have the same phylogenetic signal (Blomberg's K) as in *A*. *D*, Effect size of the regression of y on x, shown for the original dataset (orange), a set of 1000 ordinary permutations (light grey), and a set of 1000 phylogenetic permutations (black borders). The observed effect size is significantly greater than for the set of ordinary permutations, but appears

to be typical or even fairly low among the set of phylogenetic permutations. The combination of this synthetic phylogeny and the data simulated on it tend to produce strong associations, and the observed relationship is not distinguishable from those.

Predation

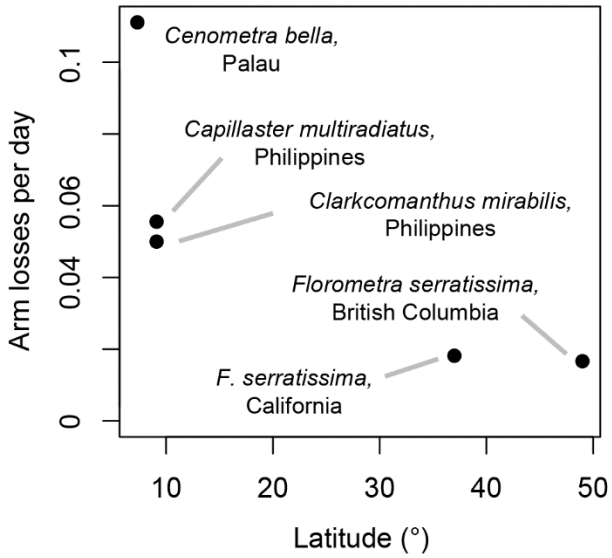

Fig. A14. Predator encounter rates for 5 shallow-water featherstar populations across latitude. Encounter rates estimated from growth rates and cross-sectional data on arm regeneration within populations. This dataset is available in the supplementary files.

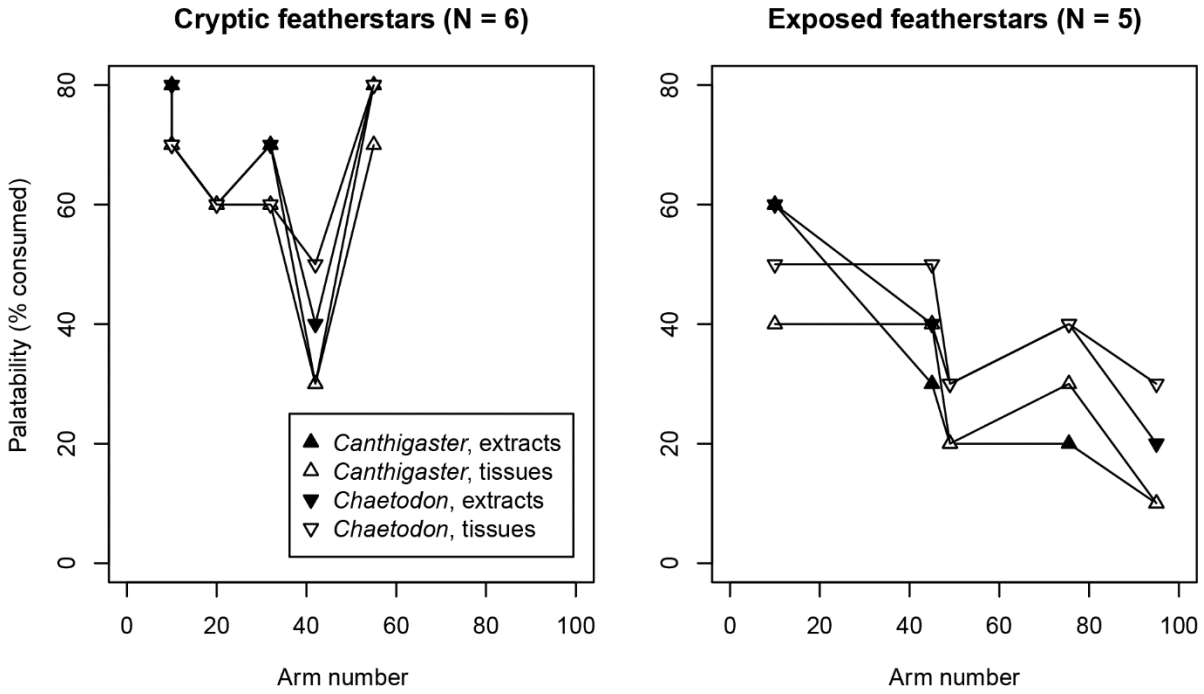

Fig. A15. Palatability of 11 species against arm number in experimental studies of consumption of crinoid tissues and extracts by the reef fish *Canthigaster* and *Chaetodon*. Lines connect data points within the same treatment.

Supplementary files

Arm number dataset

Includes 442 species with the following fields: species name, family, subfamily or tribe (for members of the Comatulidae), number of occurrences in the Ocean Biogeographic Information System, latitudinal midpoint, northernmost latitude, southernmost latitude, minimum depth (OBIS), maximum depth (OBIS), minimum depth (WoRMS), maximum depth (WoRMS), minimum depth (overall), maximum depth (overall), arm number, source for arm number, habit [from Schneider (1988); 1, diurnal exposed; 2, diurnal semi-cryptic; 3, nocturnal exposed; 4, nocturnal semi-cryptic], mean number of arms regenerating per individual [from Schneider

(1988)], mean number of arms regenerating per individual as a proportion of the total number of arms examined [from Schneider (1988)], the proportion of individuals in a species with regenerating arms [from Schneider (1988)], the number of individuals examined by Schneider (1988), and palatability (percent consumed) of crinoid extracts and tissues when presented to the tropical reef fish *Canthigaster* and *Chaetodon* as measured by Slattery (2010). The sources from which arm number data were censused are:

Clark, A. H. 1908. Descriptions of new species of recent unstalked crinoids from the coasts of northeastern Asia. Proc. U.S. Nat. Mus. 33:69–84.

Clark, A. H. 1967. A monograph of the existing crinoids. Volume 1 - the comatulids. Parts 1-5. Bulletin (United States National Museum) 82.

Fujita, Y., and M. Obuchi. 2012. Comanthus kumi, a new shallow-water comatulid (Echinodermata: Crinoidea: Comatulida: Comasteridae) from the Ryukyu Islands, Japan. Zootaxa 261–268.

Messing, C. 1998. Revision of the Recent Indo-West Pacific comatulid genus Comaster Agassiz. Part 1. The type species of Comaster and Phanogenia Lov□n (Echinodermata : Crinoidea : Comasteridae). Invertebrate Taxonomy 12.

Messing, C. G. 1995. Alloeocomatella, a new genus of reef-dwelling feather star from the tropical Indo-West Pacific (Echinodermata: Crinoidea: Comasteridae). Proceedings of the Biological Society of Washington 108:436–450.

Rowe, F. W. E., A. K. Hoggett, R. A. Birtlest, and L. L. Vail. 1986. Revision of some comasterid genera from Australia (Echinodermata: Crinoidea), with descriptions of two new genera and nine new species. Zoological Journal of the Linnean Society 86:197–277.

Predator encounter rate

The dataset used to generate Fig. A14 in the main text is included as a .xlsx file.

Phylogenies

Supplementary files include the maximum-likelihood phylogeny of featherstars, a chronogram generated using penalized likelihood with $\lambda = 0$, and the tree used in exploring the performance of phylogenetic permutations with Felsenstein's "worst case" scenario.

183

184 *R code*

185 All code needed to run analyses and generate select figures is provided in a supplementary file.

186

187 **References**

188 Cohen, K., S. Finney, P. Gibbard, and J. Fan. 2013. The ICS International Chronostratigraphic
189 Chart. Episodes 36.

190 Felsenstein, J. 1985. Phylogenies and the Comparative Method. The American Naturalist 125:1–
191 15.

192 Gislen, T. 1934. A reconstruction problem: Analysis of fossil comatulids from N. America with a
193 survey of all known types of comatulid arm-ramifications.

194 Hess, H., and C. G. Messing. 2011. Treatise on Invertebrate Paleontology, Part T, Echinodermata
195 2, revised, Crinoidea Volume 3 (W. I. Ausich ed.). Lawrence: The University of Kansas
196 Paleontological Institute.

197 Sanderson, M. J. 2002. Estimating absolute rates of molecular evolution and divergence times: A
198 penalized likelihood approach. Molecular Biology and Evolution 19:101–109.

199 Saulsbury, J., and S. Zamora. 2019. The nervous and circulatory systems of a Cretaceous crinoid:
200 preservation, paleobiology, and evolutionary significance. Palaeontology 1–11.

201 Schneider, J. 1988. *Evolutionary ecology of post-Paleozoic crinoids*. University of Cincinnati.

202 Slattery, M. 2010. Bioactive compounds from echinoderms: Ecological and evolutionary
203 perspectives. Pages 591–600 *in* L. G. Harris, S. A. Boetger, C. W. Walker, and M. P. Lesser, eds.
204 Echinoderms: Durham - Proceedings of the 12th International Echinoderm Conference. Taylor &
205 Francis Group, London, UK.

206 Smith, S. A., and B. C. O'Meara. 2012. TreePL: Divergence time estimation using penalized
207 likelihood for large phylogenies. Bioinformatics 28:2689–2690.
208 Spalding, M. D., H. E. Fox, G. R. Allen, N. Davidson, Z. A. Ferdaña, M. Finlayson, B. S.
209 Halpern, et al. 2007. Marine Ecoregions of the World: A Bioregionalization of Coastal and Shelf
210 Areas. BioScience 57:573–583.
211 Taylor, K. H. 2015. *A Phylogenetic Revision of Superfamily Himerometroidea (Echinodermata:*
212 *Crinoidea). Unpublished dissertation, Nova Southeastern University*. Nova Southeastern
213 University.
214